J Physiol 588.9 (2010) pp 1435–1449

The Journal of Physiology

Zinc inhibition of monomeric and dimeric proton channels suggests cooperative gating

Boris Musset[1], Susan M. E. Smith[2], Sindhu Rajan[3], Vladimir V. Cherny[1], Sukrutha Sujai[2], Deri Morgan[1] and Thomas E. DeCoursey[1]

[1]*Department of Molecular Biophysics and Physiology, Rush University Medical Center, Chicago, IL 60612, USA*
[2]*Department of Pathology, Emory School of Medicine, Atlanta, GA 30322, USA*
[3]*Department of Medicine, University of Chicago, Chicago, IL 60637, USA*

Voltage-gated proton channels are strongly inhibited by Zn^{2+}, which binds to His residues. However, in a molecular model, the two externally accessible His are too far apart to coordinate Zn^{2+}. We hypothesize that high-affinity Zn^{2+} binding occurs at the dimer interface between pairs of His residues from both monomers. Consistent with this idea, Zn^{2+} effects were weaker in monomeric channels. Mutation of His^{193} and His^{140} in various combinations and in tandem dimers revealed that channel opening was slowed by Zn^{2+} only when at least one His was present in each monomer, suggesting that in wild-type (WT) H_V1, Zn^{2+} binding between His of both monomers inhibits channel opening. In addition, monomeric channels opened exponentially, and dimeric channels opened sigmoidally. Monomeric channel gating had weaker temperature dependence than dimeric channels. Finally, monomeric channels opened 6.6 times faster than dimeric channels. Together, these observations suggest that in the proton channel dimer, the two monomers are closely apposed and interact during a cooperative gating process. Zn^{2+} appears to slow opening by preventing movement of the monomers relative to each other that is prerequisite to opening. These data also suggest that the association of the monomers is tenuous and allows substantial freedom of movement. The data support the idea that native proton channels are dimeric. Finally, the idea that monomer–dimer interconversion occurs during activation of phagocytes appears to be ruled out.

(Resubmitted 5 February 2010; accepted after revision 12 March 2010; first published online 15 March 2010)

Corresponding author T. E. DeCoursey: 1750 West Harrison, Chicago, IL 60612, USA. Email: tdecours@rush.edu

Abbreviations g_H, proton conductance; g_H–V, proton conductance–voltage relationship; H_V1, human proton channel protein; $H_V1\Delta C$, C-terminal truncation of H_V1; mVSOP, mouse proton channel; mVSOPΔNΔC, N- and C-terminal truncation of mVSOP; τ_{act}, activation time constant; τ_{tail}, deactivation (tail current) time constant; VSD, voltage-sensing domain.

Introduction

Human (H_V1) and mouse (mVSOP) voltage-gated proton channels in heterologous expression systems appear to function as dimers, with a conduction pathway in each monomer (Koch *et al.* 2008; Lee *et al.* 2008; Tombola *et al.* 2008). Very recent studies suggest that the monomers interact during gating, although the details of this interaction remain obscure (Gonzalez *et al.* 2010; Tombola *et al.* 2010). It is not certain that the native channel is a dimer, because dimerization has been demonstrated only in heterologous expression systems, and the gating of expressed and native proton channels differs significantly (Musset *et al.* 2008). Here we compare certain properties of monomeric and dimeric proton channels in an attempt to gain insight into possible interactions. We also focus on Zn^{2+} binding sites in the channel, which provide clues about the possible dimer interface.

The most potent inhibitor of voltage-gated proton channels is Zn^{2+} (Mahaut-Smith, 1989). The effects of Zn^{2+} are profoundly attenuated at low pH_o (Cherny & DeCoursey, 1999). This strong competition between H^+ and Zn^{2+} for an external metal binding site in native proton channels could not be explained by simple 1:1 binding. Instead, the data were well described by models that assumed that the Zn^{2+} atom was coordinated between two to three titratable groups with pK_a 6–7, suggestive of His residues (Cherny & DeCoursey, 1999). When the human proton channel gene was identified, the H_V1 protein displayed two His residues accessible to the

DOI: 10.1113/jphysiol.2010.188318

extracellular solution (Ramsey *et al.* 2006). Mutating either of these His to Ala (H140A, His^{140} replaced by Ala, or H193A, His^{193} replaced by Ala) reduced Zn^{2+} inhibition, and the double mutant had little Zn^{2+} sensitivity (Ramsey *et al.* 2006). One might conclude that Zn^{2+} inhibits proton current by binding simultaneously to His^{140} and His^{193}. However, examination of a homology model of the proton channel structure (Fig. 1*A*) reveals a striking problem, namely that the two His residues are 14 Å apart – too far to coordinate a Zn^{2+} atom by overlap of their individual electron orbitals. Analysis of Zn^{2+} binding sites in 111 proteins revealed distances of 1.9–2.4 Å between Zn^{2+} and its coordinating atom (Alberts *et al.* 1998). Of course, Zn^{2+} binding to the proton channel is rapidly reversible, and a formal binding site is not expected. No plausible alternative sequence alignment, coordinate reassignment or torsioning of His sidechains resulted in a significantly shorter distance between His residues within the monomer.

This dilemma can be resolved by postulating that Zn^{2+} binds at the interface between the two monomers (Fig. 1*B*) to complementary His resides from each monomer. Binding between residues in different subunits can occur because the corresponding His residues approach more closely than is possible in a monomer. Thus, in the dimer model shown in Fig. 1*B*, the His^{193} of the two monomers are 5.7 Å apart and the His^{140} are 9.4 Å apart. In the His–Zn–His complex, the Zn–His distance would be somewhat larger than half of these distances, depending on the coordination angle (Alberts *et al*. 1998). Thus, both pairs of His residues form potential Zn^{2+} binding sites, particularly if Zn^{2+} binding pulls the two His towards each other. Empirically, both His residues contribute to Zn^{2+} effects, because both single mutants exhibited reduced, but still significant Zn^{2+} sensitivity (Ramsey *et al.* 2006). An alternate arrangement of the monomers in the dimer results in two identical Zn^{2+} binding sites, each comprising His^{140} and His^{193}, one from each monomer (not shown). To obtain information about the Zn^{2+} binding site(s) on the human H_V1 proton channel, we generated mutants in which His^{140} and His^{193} were modified singly or together, as well as tandem dimers with various combinations of mutations.

One way to test the novel idea that Zn^{2+} binds simultaneously to His residues in the two individual monomers is to express the channel in monomeric form. The Zn^{2+} sensitivity of the monomeric channel should be identical to that of the dimer if Zn^{2+} were coordinated between the His^{140} and His^{193} within each monomer. However, if Zn^{2+} is preferentially coordinated between two His residues, one on each monomer, then the monomeric channel should have reduced Zn^{2+} sensitivity. To study monomeric human proton channels, we used a construct of H_V1 that terminated at Lys^{221} ($H_V1\Delta C$), and thus lacked the intracellular C-terminus. Coiled-coil interactions in the C-terminus stabilize the dimeric form of the channel (Lee *et al.* 2008; Tombola *et al.* 2008). To generate monomeric mouse proton channels, we truncated both C- and N-termini of mVSOP (Koch *et al.* 2008), to produce mVSOPΔCΔN. These truncations result in monomeric, but fully functional, voltage-gated proton channels, confirming that each monomer contains its own conduction pathway (Koch *et al.* 2008; Tombola *et al.* 2008). Since Zn^{2+} effects in monomeric channels were weaker, we pursued the idea that Zn^{2+} may prevent opening by constraining movement of the monomers relative to each other. A comparison of the kinetics and temperature dependence of gating of monomers and dimers, suggests that channel opening is more complex in the dimer.

Methods

Electrophysiology

In some studies, green fluorescent protein (GFP)-tagged proton channels were studied. More often, GFP was co-transfected with the proton channel construct. Fluorescent cells were identified in the field using Nikon inverted microscopes with fluorescence capability. Micropipettes were pulled using a Flaming Brown automatic pipette puller (Sutter Instruments, San Rafael, CA, USA) from 7052 glass (Garner Glass Co., Claremont, CA, USA), coated with Sylgard 184 (Dow Corning Corp., Midland, MI, USA), and heat polished to a tip resistance ranging typically from 5 to 15 MΩ with the pipette solutions used. Electrical contact with the pipette solution was achieved by a thin sintered Ag–AgCl pellet (In Vivo Metric Systems, Healdsburg, CA, USA) attached to a Teflon-encased silver wire, or simply a chlorided silver wire. A reference electrode made from a Ag–AgCl pellet was connected to the bath through an agar bridge made with Ringer solution. The current signal from the patch clamp (EPC-9 from HEKA Elektronik, Lambrecht/Pfalz, Germany, or Axopatch 200B from Axon Instruments, Foster City, CA, USA) was recorded and analysed using Lab View, SCB-68 (National Instruments, Austin, TX, USA), Pulse and PulseFit (HEKA), or pCLAMP (Molecular Devices, Sunnyvale, CA, USA) software supplemented by Microsoft Excel, Origin 7, and Sigmaplot (SPSS Inc., Chicago, IL, USA). Seals were formed with Ringer solution (in mM: 160 NaCl, 4.5 KCl, 2 $CaCl_2$, 1 $MgCl_2$, 5 Hepes, pH 7.4) in the bath, and the potential zeroed after the pipette was in contact with the cell. No liquid junction potential correction was applied.

Inside-out patches were made by forming a seal and then lifting the pipette into the air briefly. For whole-cell recording, bath and pipette solutions contained 100–200 mM buffer, 1–2 mM $CaCl_2$ or $MgCl_2$ (pipette solutions were Ca^{2+} free), 1–2 mM

EGTA, and tetramethylammonium methanesulfonate or *N*-methyl-D-glucamine to adjust the osmolality to roughly 300 mOsm, titrated with tetramethylammonium hydroxide or methanesulfonic acid. Buffers used at various pH values were Mes at pH 5.5–6.0, BisTris at pH 6.5, Pipes at pH 7.0 and Hepes at pH 7.5–8.0. We omitted EGTA from solutions for Zn^{2+} measurements. No leak correction has been applied to any current records. Except where noted, measurements were done at 21°C or at room temperature (20–25°C). The bath temperature was controlled by a system from Brooks Industries (Lake Villa, IL, USA), or by an in-house built system using Peltier devices in a feedback arrangement, monitored by a resistance temperature detector element (Omega Scientific, Stamford, CT, USA) immersed in the bath. Temperature changes were transmitted to the glass recording chamber through a supporting copper plate. The temperature probe was positioned as near the pipette tip as possible.

Currents were fitted to a rising exponential to obtain the activation time constant (τ_{act}) and the proton conductance (g_H), which was calculated from the steady-state current (the fitted current extrapolated to infinite time) using reversal potentials (V_{rev}) measured in each solution in each cell. In these fits, we ignored the initial delay in WT activation; the remaining current usually fitted a single exponential well (Fig. 3). The reversal potential (V_{rev}) was measured by two methods. When V_{rev} was negative to the threshold voltage at which the proton conductance (g_H) was first activated, $V_{threshold}$, V_{rev} was determined by the tail current method (Hodgkin & Huxley, 1952). If V_{rev} was within the range of active proton conductance, it was determined by interpolation between time-dependent inward or outward currents during test pulses (after scaling according to the tail current amplitude). The magnitude of the shift of the g_H–V relationship was determined by plotting g_H values semilogarithmically against voltage (e.g. Fig. 8), and then shifting the g_H–V relationships along the voltage axis until they superimposed upon the control curve.

With overexpression of channels in small cells, large proton currents remove enough protons from the cell to increase pH_i substantially (DeCoursey, 1991; Kapus *et al.* 1993; Demaurex *et al.* 1993; DeCoursey & Cherny, 1994, 1995, 1998; Musset *et al.* 2008; Kuno *et al.* 2009). As proton channel gating kinetics depends strongly on pH, proton

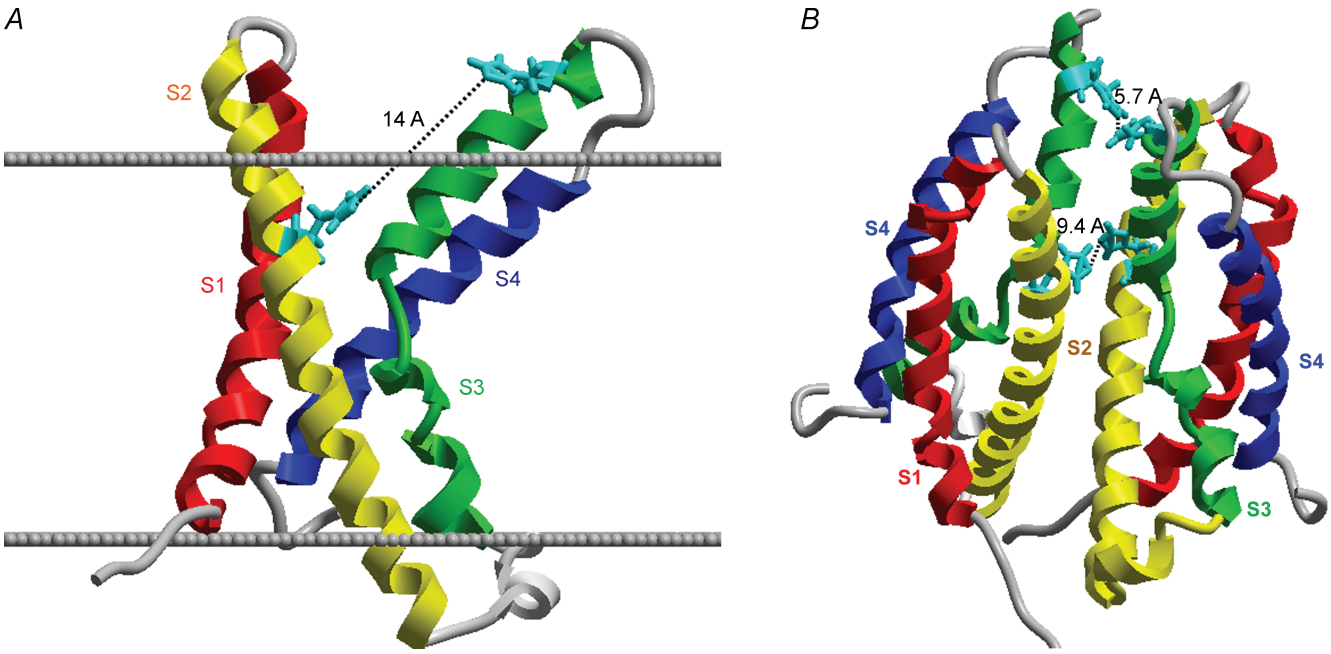

Figure 1. Homology models of the H_V1 proton channel as a monomer (*A*) or a dimer (*B*), showing the locations of the two His residues exposed to the extracellular solution
In *A*, the extracellular surface of the membrane is indicated by the upper line, the intracellular surface by the lower line. His^{140} and His^{193} are shown in aqua. In the monomer, His^{140} and His^{193} are 14 Å apart, too far to plausibly coordinate a Zn^{2+} atom. In the dimer (*B*), the His^{140} from each monomer are closer together, as are the His^{193}; either or both could comprise high-affinity Zn^{2+} binding sites. Thus, a high-affinity Zn^{2+} binding site exists only in the dimer. The recent identification of proton channel genes allows homology-based structural predictions, because the proton channel molecule bears striking homology to the voltage-sensing domain of K^+ and other voltage-gated ion channels (Ramsey *et al.* 2006; Sasaki *et al.* 2006). H_V1 contains four transmembrane domains resembling S1–S4 of other channels, but lacks the S5–S6 regions that comprise the ion conduction pathway in other channels.

depletion is a significant source of error. To minimize this problem, we applied pulses of different length to encompass different voltage ranges (Fig. 2). Longer pulses gave information about small depolarizations, and shorter pulses were used at large depolarizations, where activation was faster. Values for τ_{act} obtained in one cell for pulses of different lengths are plotted in the inset of Fig. 2. It is evident that despite a long interval between pulses, depletion progresses during families of pulses. Since cells survive a finite time and it is desirable to acquire data at multiple Zn^{2+} concentrations, some compromise is required between full pH_i recovery between pulses and ideal data. We applied infrequently repeated small test pulses after each family to determine when pH_i recovery was complete. Experiments were conducted with the intent of minimizing depletion, but also with the expectation that any systematic errors would apply equally to all constructs studied.

The slowing of τ_{act} by Zn^{2+} was evaluated over a wide voltage range, and each value was an average of the ratio at several voltages. The slowing by Zn^{2+} is roughly independent of voltage (Cherny & DeCoursey, 1999). We gave preference to τ_{act} from longer pulses, when data with different length pulses were available. As the τ_{act} *vs.* voltage relationship is often non-monotonic, with smaller values near $V_{threshold}$ that first increase and then decrease with depolarization (Musset *et al.* 2008), as evident in Fig. 2, we compared values positive to the maximum τ_{act} value.

Except where noted, statistical comparisons used Student's unpaired *t* test.

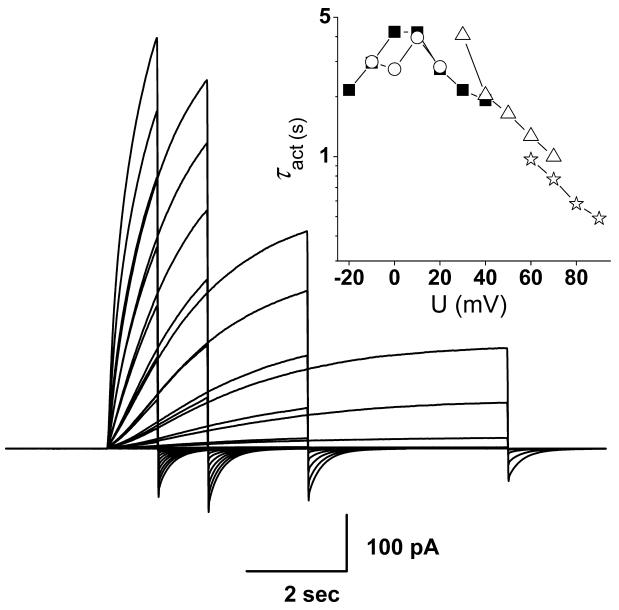

Figure 2. Use of different pulse lengths to evaluate τ_{act} at different voltage ranges, to minimize distortion of kinetics by proton depletion
Superimposed are four pulse families of different durations in the same cell, transfected with the H193A–H140A tandem dimer at pH_o 7.0, pH_i 6.5 with 10 μM Zn^{2+}. Pulses were applied in increasingly positive steps in 10 mV increments from a holding potential of −60 mV up to +20 mV (8 s pulses, ○), +40 mV (4 s, ■), +70 mV (2 s, △) or +90 mV (1 s, ☆). Pulses were applied at 22 s intervals except for a 38 s interval for the 8 s family. The order of families was 4 s, 8 s, 2 s and 1 s. The inset shows τ_{act} estimated from these records.

Culture, mutation and transfection

HEK-293 cells were maintained in 5% CO_2 and 95% air in a humidified incubator at 37°C in Dulbecco's modified Eagle's medium containing 10% heat-inactivated fetal bovine serum, 2 mM L-glutamine, 100 U ml^{-1} penicillin, 250 ng ml^{-1} Fungizone and 100 μg ml^{-1} streptomycin. The coding sequence of human H_V1 (*Hvcn1*) was cloned into either pcDNA3.1(–) or pQBI25-fC3 (to make GFP–H_V1) vectors as described previously (Ramsey *et al.* 2006). The mouse orthologue (mVSOP) was derived from RIKEN cDNA 0610039P13 as described previously (Sasaki *et al.* 2006). HEK-293 cells were grown to ∼80% confluency in 35 mm cultures dishes, usually by seeding cells 1 day ahead of transfection. Cells were transfected in media without fetal bovine serum with ∼0.7 μg of the appropriate cDNA using Lipofectamine 2000 (Invitrogen). After 6 h incubation at 37°C in 5% CO_2, the medium was replaced with medium containing fetal bovine serum. The next day, the cells were trypsinized and re-plated onto glass coverslips at low density for patch clamp recording. We selected green cells under fluorescence for recording.

The C-terminus of mouse mVSOP was truncated by introducing a stop codon at K217 (Quikchange site directed mutagenesis kit, Stratagene, San Diego, CA, USA). For N- and C-terminal truncations, mVSOP was amplified with primers containing a start codon at T77 and a stop codon at K217, and the PCR product was cloned in pCDNA 3.1(+). Single mutations, H140A and H193A, were generated by site-directed mutagenesis. The WT–WT, H193A–H140A and WT–H140A/H193A tandem constructs were made by removing the stop codon in the respective constructs in pCDNA and introducing a *Nhe*1 site and three alanines forming a six amino acid linker, ASGAAA, between the two proteins.

Homology model

A homology model of the voltage-sensing domain (VSD) of human H_V1 (NCBI NP_115745.2) was created using Insight II (Accelrys, San Diego, CA, USA). The basis set consisted of the isolated voltage sensor of KvAP (1ORS) and the voltage sensor of Kv1.2 (2R9R) (Jiang *et al.* 2003*a*; Long *et al.* 2007). Basis set crystal structures were structurally aligned, and the sequence of the human H_V1 VSD was aligned to a structure-based sequence alignment in BioEdit (Ibis Biosciences). Direct

coordinate assignment was performed on structurally conserved regions. Loop assignments were performed via loop searches using a local subset of the Protein Data Bank, and using the Archpred server (Fernandez-Fuentes *et al*. 2006). Energy minimization routines were run to convergence on the splice points, the loops and the side-chains of the structurally conserved regions. In the final model, Procheck (Laskowski *et al.* 1993) revealed very few unrealistic bond lengths and bond angles, all of which resulted from crystal-based assignments. The general features of this model, including the distance between His^{140} and His^{193}, were supported by an independent model generated using the automated I-TASSER method (Zhang, 2008).

Monomer models were visualized in Insight and in MolSoft ICM Pro (MolSoft), and the two monomers were moved manually ('visual docking'), to verify the plausibility of Zn^{2+} binding between monomers. Further support for plausible Zn^{2+}-binding dimer configurations was sought by submitting the model to the GrammX protein–protein docking server (Tovchigrechko & Vakser, 2006), using the homodimer option and with varying numbers of residues suggested as participating in the interface. Results of docking runs were initially visualized and inspected in VMD (visual molecular dynamics) (Humphrey *et al.* 1996). Dimer models retained from initial inspections were superimposed on a model of the 2R9R crystal structure in the plasma membrane obtained from the Orientations of Proteins in Membranes database (Lomize *et al*. 2006) to assess their ability to span the membrane appropriately. Approximately 1% of the dimers returned from the docking runs were in realistic orientations. Figure 1*B* is a representative example from the realistic dimers that were identified, all of which had His–His distances of 4–10 Å.

Results

Activation kinetics in monomeric and dimeric proton channels

The activation kinetics of monomeric and dimeric proton channel currents differs in two respects. First, WT dimeric proton channels activate with a sigmoidal time course (Fig. 3*A*), like all native proton currents (DeCoursey, 2003). In contrast, monomeric $H_V1\Delta C$ proton currents activate with an exponential time course (Fig. 3*B*). We fitted all currents to a single rising exponential to obtain the time constant of activation, τ_{act}. For dimeric channel currents, we ignored the initial delay. Exponential opening is consistent with a simple first order opening transition in the monomer. Sigmoidal kinetics can be explained by a cooperative gating process in which multiple subunits must undergo an opening transition before conduction can occur (Hodgkin & Huxley, 1952). As the proton channel is a dimer in which each monomer contains its own conduction pathway (Koch *et al.* 2008; Tombola *et al.* 2008; Lee *et al*. 2008), such cooperativity is surprising.

Consistent with previous reports (Koch *et al.* 2008; Tombola *et al.* 2008), channel opening in $H_V1\Delta C$ or mVSOPΔNΔC monomers was much faster than in WT dimers (Fig. 3, and not shown). Inside-out patches were used for this measurement, because proton depletion notoriously can distort gating kinetics in whole-cell studies (DeCoursey, 1991; Kapus *et al.* 1993; Demaurex *et al.* 1993; DeCoursey & Cherny, 1994, 1995, 1998; Musset *et al.* 2008; Kuno *et al.* 2009). The average ratio of τ_{act} in $H_V1/H_V1\Delta C$ measured (at each voltage) in inside-out patches at pH_o 7.5, pH_i 7.5 at +30 to +80 mV in 10 mV increments was 6.58 ± 0.44 (mean ± S.E.M. for 6 voltages, each with 4–7 cells for H_V1 and 5–7 cells for $H_V1\Delta C$).

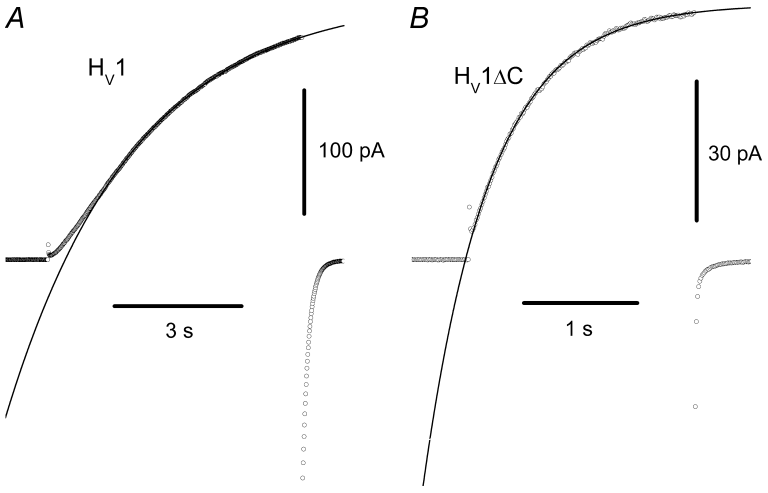

Figure 3. WT dimeric proton channels open slowly with a sigmoidal time course (*A*), but monomeric $H_V1\Delta C$ channels open rapidly and exponentially (*B*)
Individual current records are shown at +50 mV from a holding potential of −40 mV in inside-out patches at pH_o 7.5, pH_i 7.5 at 23°C. Single exponential fits are superimposed and extrapolated on the data points shown as circles. For the records shown here, τ_{act} was 3.0 s and 0.59 s for WT and $H_V1\Delta C$, respectively.

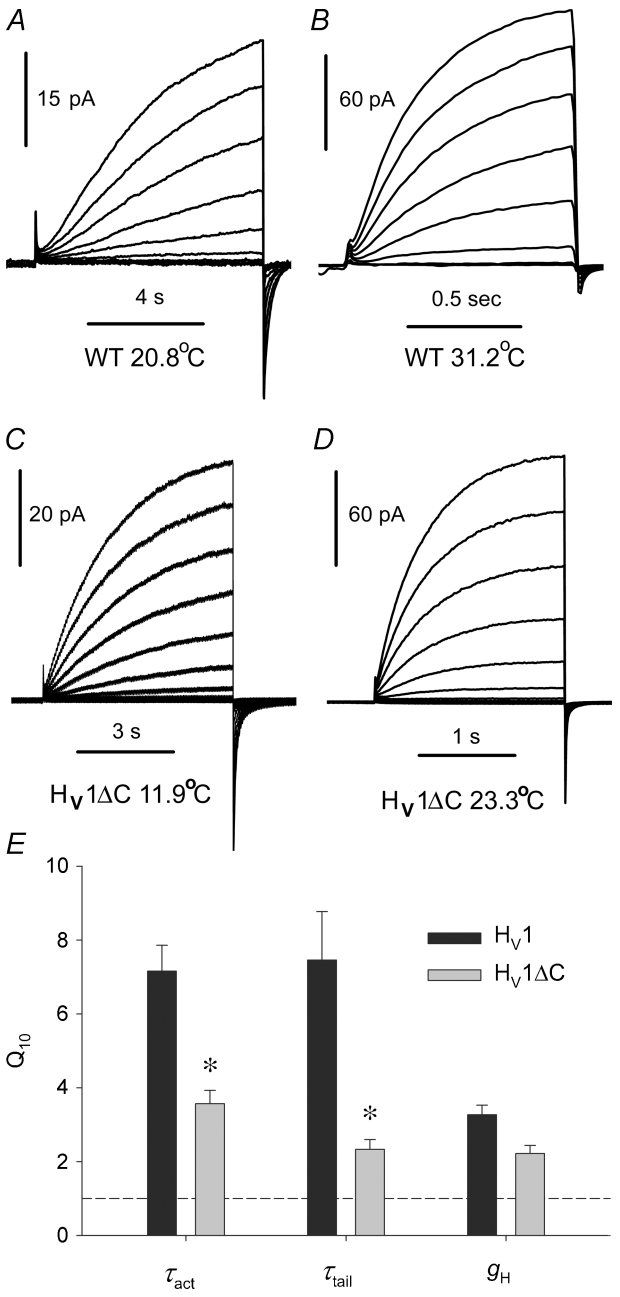

Figure 4. Temperature dependence of WT (*A* and *B*) and H$_V$1ΔC proton currents (*C* and *D*) recorded in inside-out patches of membrane

For each patch, families of pulses to the same voltages were applied, with the pulse duration adjusted as shown. *A*, WT proton currents during pulses from −60 mV to +20 mV in 10 mV increments at 20.8°C (*A*) and 31.2°C (*B*), at pH$_o$ 7.5, pH$_i$ 6.5. *C*, H$_V$1ΔC proton currents in a patch elicited by families of pulses from −40 mV to +80 mV in 10 mV increments, at 11.9°C. *D*, pulses to the same voltages in the same patch at 23.3°C. Both at pH$_o$ 7.5, pH$_i$ 7.5. *E*, summary of the temperature dependence of WT and H$_V$1ΔC proton channel gating kinetics and conductance. Measurements were made in excised inside-out patches to avoid depletion effects.
Means ± S.E.M. are shown for 6–8 WT (H$_V$1) patches and 6–9 H$_V$1ΔC patches. *$P < 0.01$ by Student's *t* test.

A 5-fold slower time-to-half-peak was reported for mVSOP than mVSOPΔNΔC (Koch *et al.* 2008). Faster activation of monomeric channels suggests that interaction between monomers in the dimer slows opening or that the presence of cytoplasmic domains slows gating (Koch *et al.* 2008). Proton channels in monomeric form obligatorily gate independently; apparently a qualitatively different gating process occurs in the dimer.

Temperature dependence is weaker in the monomer

A complex gating mechanism for WT dimeric proton channels is consistent with the extreme temperature dependence of gating of native proton channels ($Q_{10} = 6$–9, or 30–38 kcal mol^{-1} for both opening and closing kinetics) (DeCoursey & Cherny, 1998). If part of the energetic barrier arises from inter-subunit interaction, the temperature dependence of gating in the monomeric construct might be weaker. Figure 4 illustrates that this was the case for the human proton channel: gating kinetics in the H$_V$1ΔC monomer had temperature dependence only about half that of wild type (WT) H$_V$1. Families of WT (*A* and *B*) and H$_V$1ΔC (*C* and *D*) proton currents are shown at roughly 10°C different temperatures. The time scales differ by a factor of 8 for WT and 3 for H$_V$1ΔC, illustrating the much stronger temperature dependence of channel opening kinetics in the dimer. We used excised, inside-out patches of membrane for these measurements to avoid complications due to proton depletion during large currents (DeCoursey & Cherny, 1998; Kuno *et al.* 2009). Estimates were based on several currents from families of pulses recorded at two or more temperatures, with the assumptions that within the error of the estimates, Q_{10} for gating kinetics is independent of voltage and pH (DeCoursey & Cherny, 1998; Kuno *et al.* 2009). On average, the Q_{10} of channel opening (τ_{act}) was 7.16 for WT and 3.57 for H$_V$1ΔC (Fig. 4*E*). The Q_{10} for channel closing (τ_{tail}, tail current time constant) was 7.46 for WT and 2.33 for H$_V$1ΔC. Measurements were made over a pH range of 5.5–7.5 and within the temperature range 9–32°C. Thus, channel opening and closing are both substantially more energetically demanding in WT dimeric channels, suggesting a different gating mechanism.

Zn^{2+} sensitivity of the monomer is weaker than the dimer

Figure 5 shows that the Zn^{2+} sensitivity of the monomeric H$_V$1ΔC channel (Fig. 5*B*) was distinctly weaker than that of the dimeric H$_V$1 (Fig. 5*A*). The main effects of Zn^{2+} on proton currents are to slow channel opening (larger activation time constant, τ_{act}) and to shift the proton conductance–voltage relationship, g_H–V, positively. The

slowing of τ_{act} was significantly greater in the WT channels than in the $H_V1\Delta C$ ($P < 0.01$ at 1, 10 and 100 μM Zn^{2+}, data not shown).

Measurements were also performed on mouse proton channels and the monomeric mVSOPΔNΔC construct, in order to determine whether the phenomena described here apply to proton currents in other species. WT mouse proton currents (mVSOP) activated sigmoidally, and the monomeric mVSOPΔNΔC currents activated exponentially (not shown). Slowing of τ_{act} by Zn^{2+} was evaluated as described for H_V1. The Zn^{2+} sensitivity of the monomeric construct was significantly weaker than WT at 1, 10 and 100 μM Zn^{2+} ($P < 0.05$ for each, data not shown).

Some slowing of activation is expected to result from the shift by Zn^{2+} of the gating of most voltage-dependent channels, although depending on the mechanism, different gating parameters may be shifted by different amounts (Frankenhaeuser & Hodgkin, 1957; Hille, 2001; Elinder & Åhrem, 2004). To evaluate this electrostatic effect, we determined the shift of the g_H–V relationship produced by each [Zn^{2+}] in each cell and shifted the τ_{act}–V relationship negatively by that amount. Figure 6 shows the residual slowing of τ_{act} after this correction. WT murine and human proton channels are slowed by Zn^{2+} beyond what is expected from a simple voltage shift, but for the mVSOPΔNΔC and $H_V1\Delta C$ constructs, most of the observed slowing was attributable to the voltage shift.

Zn^{2+} sensitivity of histidine mutants

In order to further test the hypothesis that externally applied Zn^{2+} exerts its characteristic effects at one or more high affinity binding sites at which Zn^{2+} is coordinated between two His residues on the proton channel, we studied a series of His mutants and constructs, illustrated in the diagram in Fig. 7. The various constructs in Fig. 7 were expressed and studied at pH_o 7.0 in the presence of Zn^{2+}. Of the main effects of Zn^{2+} (Cherny & DeCoursey, 1999), we focused on the shift of the g_H–V relationship (Figs 8 and 9*A*) and the slowing of τ_{act} (Fig. 9*B*).

With regard to the shift of the g_H–V relationship by Zn^{2+}, H140A was similar to WT, but H193A was distinctly less sensitive (Fig. 9*A*; $P < 0.001$ at all [Zn^{2+}]). This result suggests that Zn^{2+} bound to His^{193} exerts a stronger effect on the voltage sensor of the proton channel. Surprisingly, both single His mutants H140A and H193A exhibited more similar slowing effects (Fig. 9*B*), although H193A was again more sensitive ($P < 0.05$ *vs.* H140A at 1 and 10 μM Zn^{2+}). The slowing of τ_{act} by Zn^{2+} was significantly weaker than WT in either single mutant, indicating that both His residues contribute to the slowing of channel opening by Zn^{2+}. The double His mutant H140A/H193A

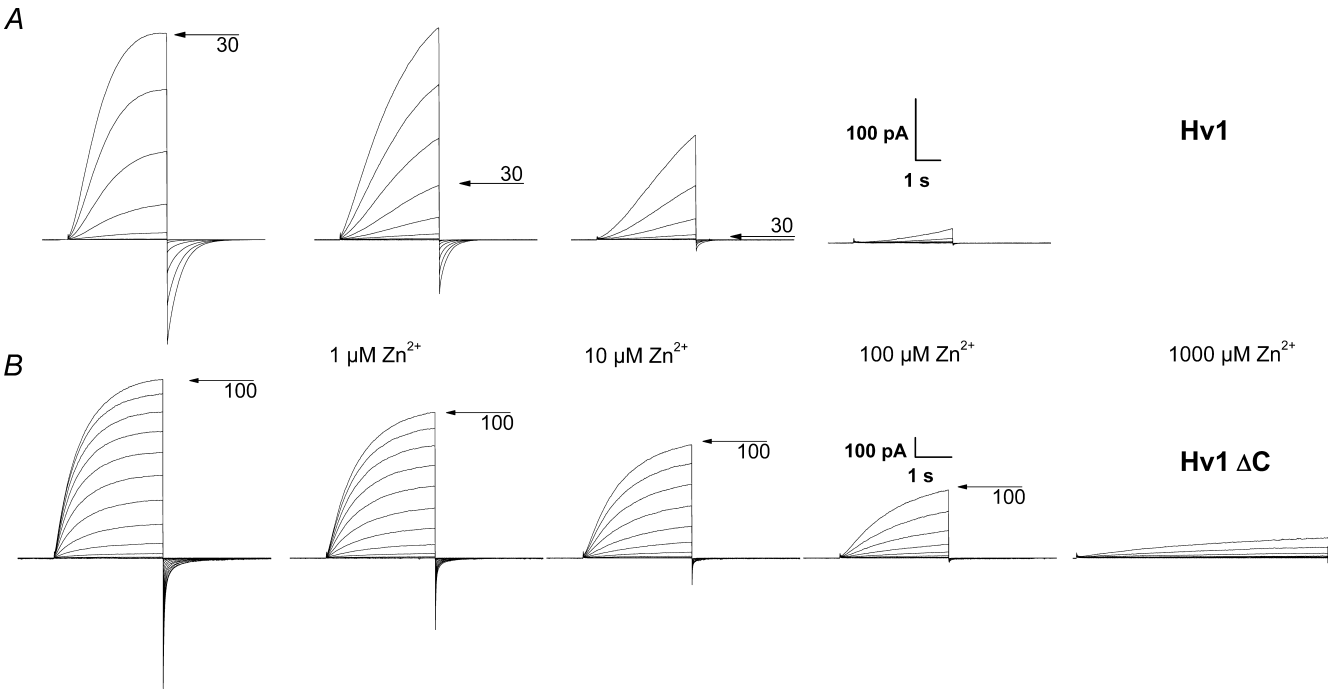

Figure 5. The Zn^{2+} sensitivity of the human monomeric proton channel is weaker than that of the dimer
A, WT H_V1 proton current families in the same cell at pH_o 7.0, pH_i 6.5 during pulses in 10 mV increments to +30 mV (control) or to +60 mV (Zn^{2+}). *B*, weaker Zn^{2+} sensitivity of $H_V1\Delta C$ monomeric channels at pH_o 7.0, pH_i 6.5. Pulses were applied in 10 mV increments up to +100 mV.

exhibited essentially no slowing by Zn^{2+}, but a weak shift of the g_H–V relationship remained. The shift may reflect non-specific divalent cation effects or Zn^{2+} binding to sites on the channel other than His. Nevertheless, that no slowing was seen in H140A/H193A suggests that virtually the entire slowing effect can be attributed to Zn^{2+} binding to His^{140} and His^{193}.

Zn^{2+} sensitivity of histidine mutants and constructs: tandem dimers

A control WT–WT tandem dimer was generated by linking two WT H_V1 channels. The gating and Zn^{2+} sensitivity of this WT–WT tandem dimer (Fig. 8*A*) were indistinguishable from WT channels. This result supports the validity of the use of tandem dimers to evaluate the characteristics of Zn^{2+} binding to H_V1. In addition, this result further supports the conclusion that the *Hvcn1* gene product assembles as a dimer in several expression systems (Koch *et al.* 2008; Lee *et al.* 2008; Tombola *et al.* 2008).

If a high-affinity binding site for Zn^{2+} can exist within a single monomer, then a high-affinity site should exist on the WT–H140A/H193A tandem dimer, which retains both His residues in one monomer but neither in the other. However, Zn^{2+} effects were drastically attenuated in this construct (Fig. 8*B*). For example, in the WT–WT tandem dimer, 1 μM Zn^{2+} already shifts the g_H–V relationship positively by ~10 mV (Fig. 8*C*). In contrast, in the WT–H140A/H193A tandem dimer, little shift occurs until 100 μM Zn^{2+} is introduced (Fig. 8*D*).

The properties of the WT–H140A/H193A tandem dimer were unique in one respect. Most of the channel constructs tested activated exponentially or exponentially after a delay, with or without Zn^{2+}. An exception is the H193A–H140A tandem dimer, whose currents were sometimes better fitted with two components in the absence of Zn^{2+}. Proton currents in the WT–H140A/H193A tandem dimer activated with two components, but only in the presence of $\geq$100 μM Zn^{2+} (Fig. 8*B*). When fitted with two exponentials, the faster component had time constants <1 s, whereas the time constant of the slower component was close to τ_{act} measured in the absence of Zn^{2+}. Thus, Zn^{2+} not only failed to slow activation, it appeared to introduce a novel rapid component of activation. Assuming that cooperative gating normally occurs, it might be speculated that in this construct, Zn^{2+} may uncouple the two monomers. In any case, the absence of slowing by Zn^{2+} of any component of opening of the WT–H140A/H193A tandem dimer suggests that slowing occurs when Zn^{2+} binds between His residues in the two monomers at the dimer interface.

The shifts of the g_H–V relationship and the slowing of τ_{act} produced by Zn^{2+} are summarized for this and other constructs in Fig. 9. Figure 9*A* reveals that the shift in the g_H–V relationship produced by Zn^{2+} was almost as weak in the WT–H140A/H193A construct which has one pair of dissimilar His residues as in the double mutant H140A/H193A that lacks His altogether.

Upon examination of the slowing of channel opening by Zn^{2+} (Fig. 9*B*), the constructs fall into three categories. Slowing is most profound for constructs in which both pairs of His^{193} and His^{140} exist (WT and WT–WT tandem). Weaker but distinct slowing also occurs when a single symmetrical pair of His^{140} or His^{193} are present (H193A or H140A) or the asymmetrical pair (H193A–H140A tandem dimer). Remarkably, there was practically no slowing of activation in the WT–H140A/H193A tandem dimer or the double mutant H140A/H193A. The simplest interpretation is that slowing occurs when Zn^{2+} can interact with both monomers simultaneously.

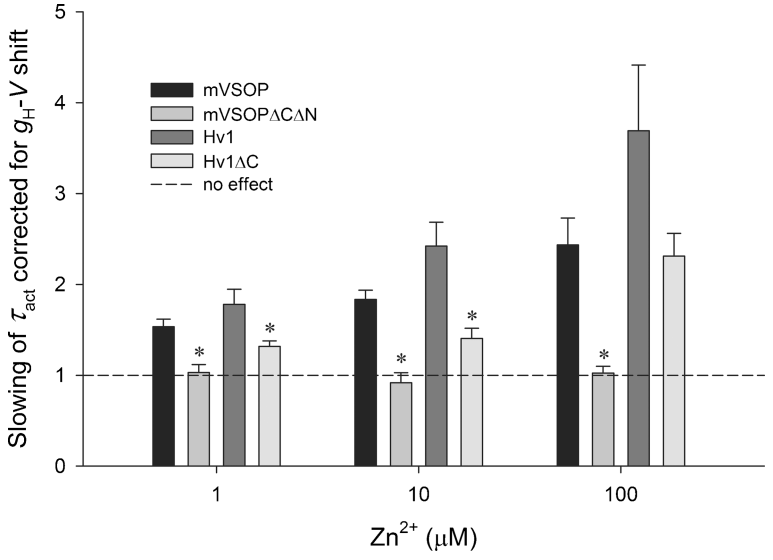

Figure 6. Monomeric proton channels (mVSOPΔNΔC or H_V1ΔC) are less sensitive to the slowing effect of Zn^{2+} than WT dimeric channels (mVSOP or H_V1)
Plotted is the mean ± S.E.M. residual slowing after correction for the observed shift of the g_H–V relationship in each cell at each [Zn^{2+}]. Slowing is defined as the ratio $\tau_{act}(Zn^{2+})/\tau_{act}$, which was determined at moderate depolarizations in the voltage range where τ_{act} is approximately exponentially dependent on voltage. For mVSOPΔNΔC and mVSOP, n = 3–4; for H_V1 and H_V1ΔC, n = 8–11. *P < 0.05 for truncated *vs.* WT channels.

Discussion

Monomer interactions during channel opening

An apparent contradiction between structural predictions based on electrophysiological measurements of competition between Zn^{2+} and H^+ (Cherny & DeCoursey, 1999), and a molecular homology model of the proton channel VSD (Fig. 1) led to the hypothesis that Zn^{2+} binds between monomers in the proton channel dimer. The obvious prediction that monomeric channels should have lower Zn^{2+} affinity was borne out. That Zn^{2+} could prevent channel opening at such a location further suggested that the two monomers are closely apposed and may interact during channel opening. Several types of evidence are consistent with this hypothesis. Monomeric channels open with an exponential time course, rather than the sigmoidal kinetics typical of all native proton channels (DeCoursey, 2003) and of cooperative gating mechanisms in general (Hodgkin & Huxley, 1952; Horrigan *et al.* 1999). Channel opening was 6.6 times faster in monomeric channels, consistent with a more facile opening process than in the dimer. The activation energy of WT channel gating was double that of monomeric channels, indicating a more complex opening process in the dimer. The native voltage-gated proton channel has much larger activation energy for opening than most other voltage-gated ion channels. That the Q_{10} was found to be similar for the delay, τ_{act} and τ_{tail}, led to the suggestion that the channel comprises multiple subunits that each undergoes a single rate-determining conformational change (DeCoursey & Cherny, 1998). Finally, Zn^{2+} retards proton channel opening beyond the slowing expected from a simple voltage shift (Cherny & DeCoursey, 1999), as was observed for Cd^{2+} effects on snail neuron proton channels (Byerly *et al.* 1984). Together, these observations strongly suggest pronounced interaction between monomers during proton channel opening. Two recent studies support this conclusion by providing evidence for cooperativity (Gonzalez *et al.* 2010; Tombola *et al.* 2010). In one proposal, both monomers must activate before either can conduct current (Gonzalez *et al.* 2010). In the other proposal, the subunits can open individually, but positive cooperativity results in both usually being in the same open or closed state (Tombola *et al.* 2010).

The physical interpretation of the present results is not clear-cut. Ascribing the delay in H^+ current activation to a gating step (between closed states) preceding opening in each (independent) monomer would not account for the absence of delay in monomeric channels. One possibility is that in the dimer, the gating of each monomer is slowed by the presence of the other monomer. Alternatively, perhaps both channel subunits must enter the 'open' configuration before either can conduct current. This interpretation is suggested by the observation that the monomeric channel activates with an exponential time course, whereas dimeric channel currents exhibit a sigmoidal time course (Fig. 3), reminiscent of classical Hodgkin–Huxley kinetics (Hodgkin & Huxley, 1952). Similarly, for the *Ciona* proton channel (CiVSOP), monomeric constructs activated exponentially, whereas the dimer opened with sigmoidal kinetics (Gonzalez *et al.* 2010). The relatively brief delay and slower subsequent activation suggest that a slow concerted gating process occurs after both monomers have activated (Horrigan *et al.* 1999). In either case, the slower activation of dimeric

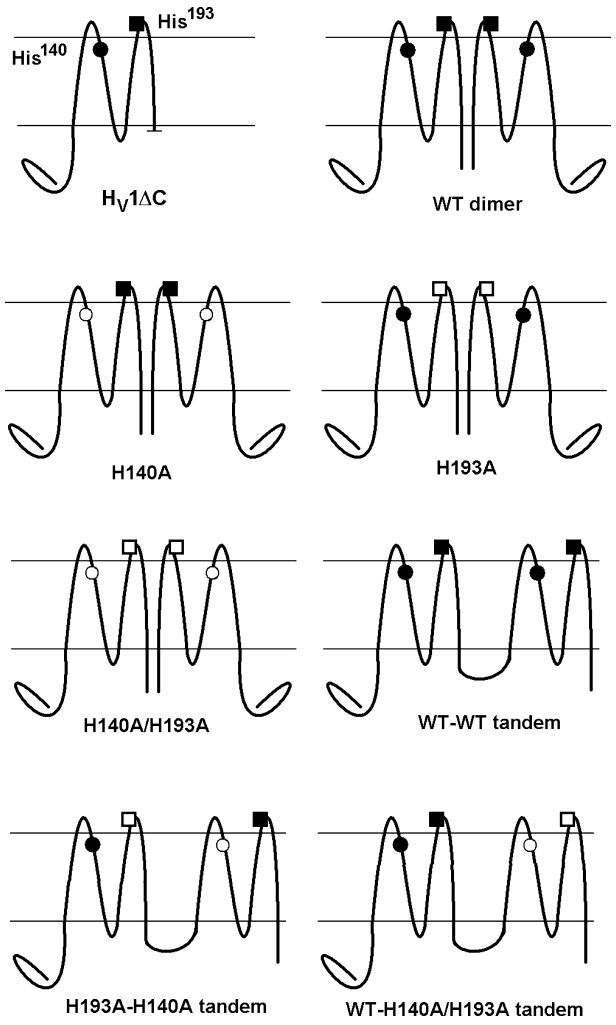

Figure 7. Diagram of the histidine mutants and constructs used and their nomenclature
His^{140} is on S2 near the external surface of the membrane; His^{193} is on the S3–S4 linker. Filled symbols indicate His, open symbols indicate Ala substitution. The C-terminal truncation $H_V1\Delta C$ expresses as a monomer (Tombola *et al.* 2008; Koch *et al.* 2008). The dimer assembles mainly by C-terminal interactions (Tombola *et al.* 2008; Koch *et al.* 2008; Lee *et al.* 2008). Tandem dimers were linked by insertion of –ASGAAA– between C- and N-termini of two monomers.

channels suggests a complex gating process involving interaction between the two monomers. Intriguingly, direct measurements of the single-channel current of voltage-gated proton channels provided estimates that were roughly twice the value determined from current fluctuation analysis (Cherny *et al.* 2003). This observation is compatible with a gating process in which both channels in the dimer open approximately synchronously often enough to be interpreted as a single opening event (with twice the unitary conductance), but in which most gating transitions (that contribute to the fluctuations) involve individual conduction pathways. This phenomenology appears to be more consistent with the proposal of Tombola *et al.* (2010) than that of Gonzalez *et al.* (2010).

The sigmoidal activation kinetics (DeCoursey, 2003) and strong temperature dependence of gating of native proton currents (DeCoursey & Cherny, 1998; Kuno *et al.* 2009) closely resemble the corresponding behaviour of expressed WT (dimeric) proton channels, but not monomeric constructs. These properties therefore support the idea that the native proton channel, like expressed proton channels, assembles as a dimer, despite the difference in voltage dependence of expressed and native proton channels (Musset *et al.* 2008).

Teleological advantages of cooperative gating

Why would cooperative gating at the expense of slower activation be advantageous for proton channels? Cooperativity increases the voltage sensitivity of channel opening (Sigworth, 1993). Proton channels exist in many non-excitable cells. In many situations that result in channel opening, speed typically is not an important consideration. For example, the phagocyte respiratory burst continues for roughly 1 min to 1 h depending on the stimulus (DeCoursey & Ligeti, 2005). It may be more important that proton channels open with steep voltage dependence than rapidly. Proton efflux limits membrane depolarization, which is desirable during the respiratory burst, because NADPH oxidase enzyme activity is voltage dependent, and is inhibited at large positive voltages (DeCoursey *et al.* 2003; Petheő & Demaurex, 2005).

Deducing channel architecture from Zn^{2+} effects

Simple models of competition between H^+ and Zn^{2+} indicated that Zn^{2+} binds to multiple titratable groups with pK_a 6.2–7.0 (Cherny & DeCoursey, 1999). The human proton channel has two His residues predicted to be exposed to the extracellular solution, His^{140} and His^{193},

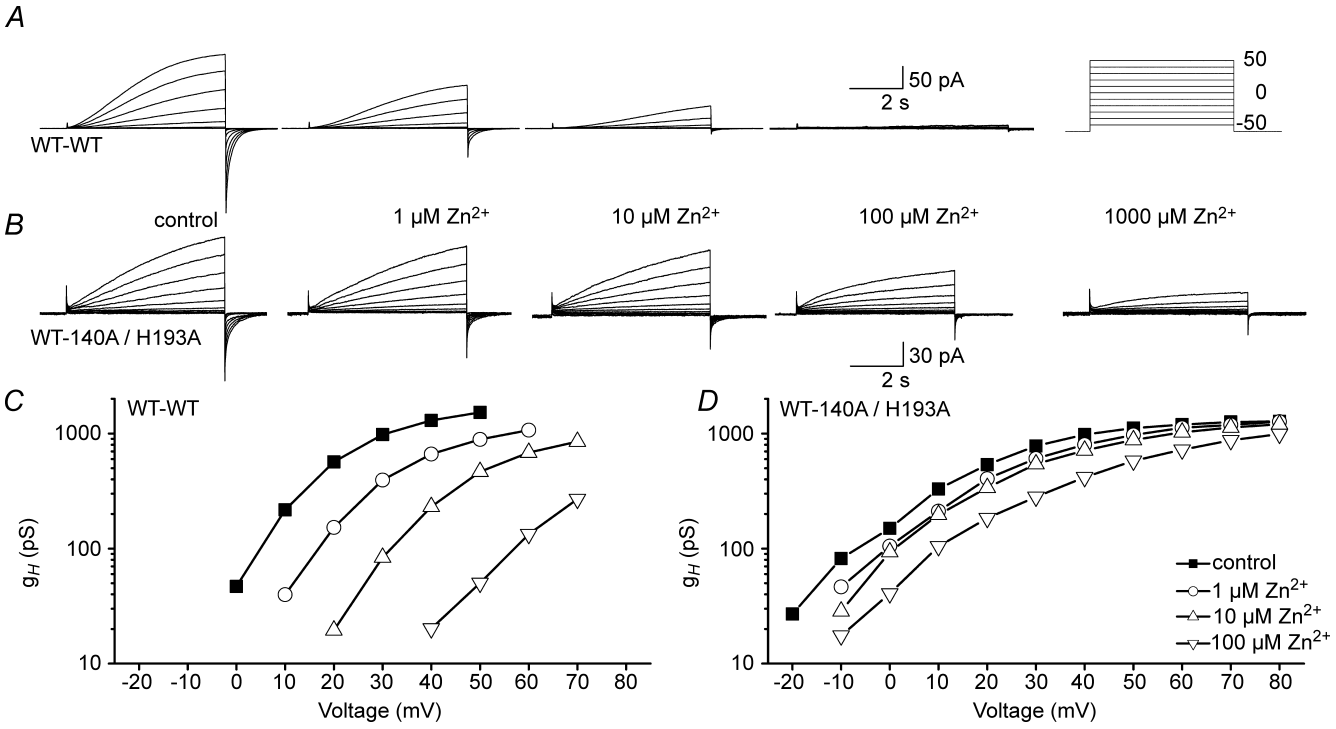

Figure 8. Greatly reduced Zn^{2+} sensitivity of the WT–H140A/H193A tandem dimer, compared with the WT–WT tandem dimer

All current families in the WT–WT tandem dimer (*A*) or the WT–H140A/H193A tandem dimer (*B*) were recorded during pulses to the voltages shown in the inset at pH_o 7.0, pH_i 6.5. *C* and *D*, the g_H–*V* relationships were determined from the cells in *A* and *B* using reversal potentials measured in each cell.

and mutation of either one to Ala reduced Zn^{2+} sensitivity of the channel; the double mutant H140A/H193A was even less sensitive (Ramsey *et al.* 2006; see also Fig. 9). These observations point to Zn^{2+} coordination between two His residues. The two His in each monomer were too far apart to coordinate Zn^{2+} in the homology model (Fig. 1*A*), and the weaker Zn^{2+} effects in monomeric $H_V1\Delta C$ are consistent with the distance between His^{140} and His^{193}

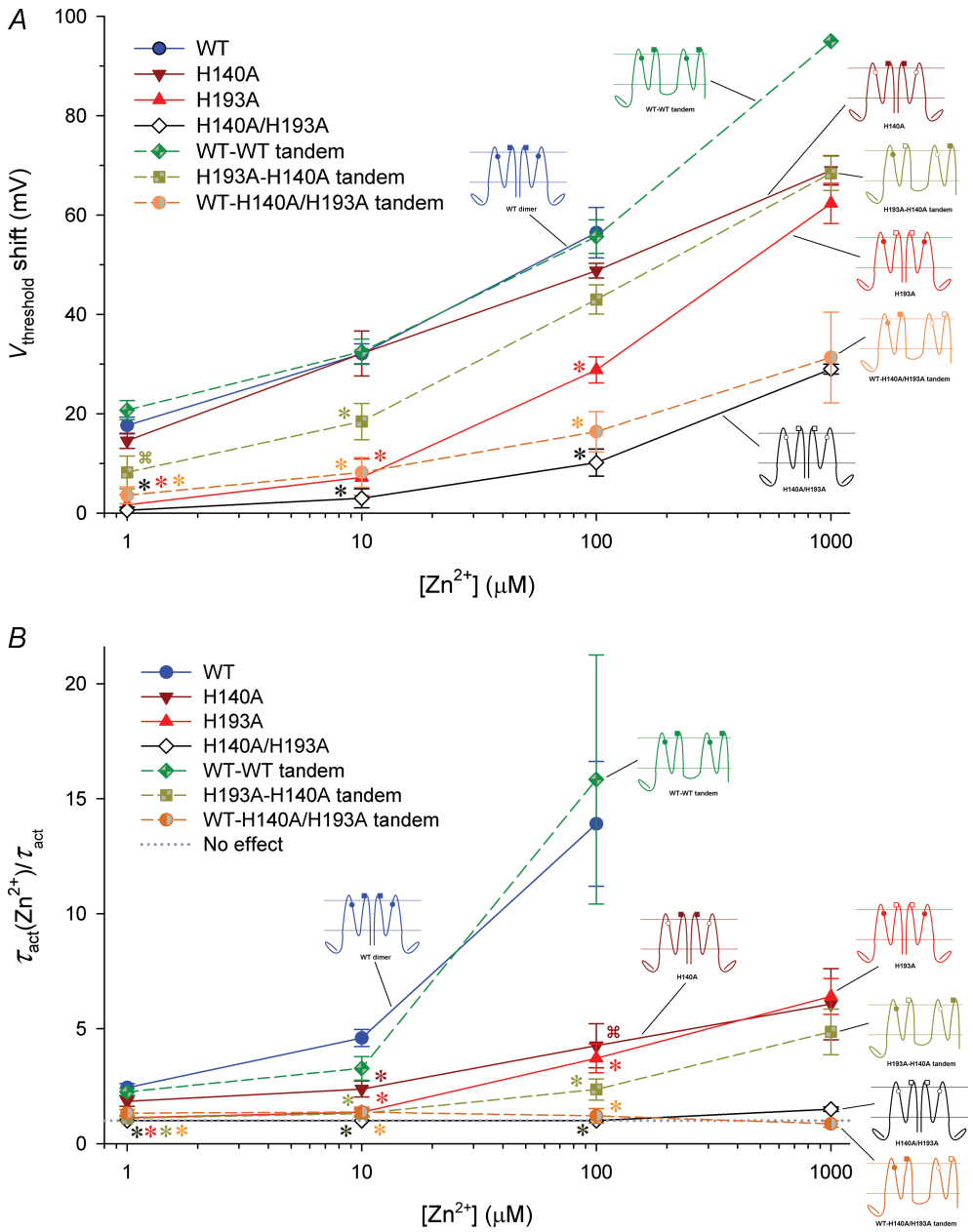

Figure 9. Effects of Zn^{2+} on the voltage dependence and gating kinetics of several proton channel constructs with His mutations

A, shifts of the g_H–*V* relationship produced by Zn^{2+} in various human H_V1 constructs. Inset diagrams illustrate the positions of His^{140} and His^{193} residues (●, ■) or their substitution by Ala (○, □), respectively, as also shown in Fig. 7. Tandem dimer data are connected by dashed lines. Mean ± S.E.M. are shown for numbers of cells studied at up to 100 μM Zn^{2+}: 9–12 WT; 5–7 H140A; 5–6 H193A; 5–6 H140A/H193A; 3–12 WT–WT tandem; 5–7 H193A–H140A tandem; 5–6 WT–H140A/H193A tandem. $^{⌘}P < 0.05$, $^{*}P < 0.01$ by Student's *t* test compared with WT. *B*, slowing of activation kinetics produced by Zn^{2+} in various H_V1 constructs. Mean ± S.E.M. slowing of τ_{act} by Zn^{2+} (defined as the ratio $\tau_{act}(Zn^{2+})/\tau_{act}$) in the indicated proton channel constructs, for numbers of cells studied at up to 100 μM Zn^{2+}: 8–11 WT; 5–7 H140A; 5–8 H193A; 4 H140A/H193A; 4–11 WT–WT tandem; 5–7 H193A–H140A tandem; 5–6 WT–H140A/H193A tandem. $^{⌘}P < 0.05$, $^{*}P < 0.01$ by Student's *t* test compared with WT.

being too great for Zn^{2+} to bind to both His within a single monomer. However, potential high-affinity Zn^{2+} binding sites occur at the interface between monomers in the dimer model. Plausible dimer models were identified in which potential binding sites were comprised of His^{140}–His^{140} or His^{193}–His^{193} pairs (Fig. 1*B*). An alternative site formed by His^{140}–His^{193} from complementary subunits can be obtained by small, opposite rotations of each monomer in the dimer shown in Fig. 1*B*, around an axis parallel to the membrane. The resulting His^{140}–His^{193} distance is approximately 7 Å (not shown).

An alternate interpretation is that in the WT channel, strong Zn^{2+} effects are the result of Zn^{2+} binding independently to each channel subunit. Two arguments oppose this interpretation. First, the competition between H^+ and Zn^{2+} required that at least two titratable groups coordinate Zn^{2+} at its primary site of action (Cherny & DeCoursey, 1999). Second, assuming that neither channel can conduct until both undergo an opening transition (Gonzalez *et al.* 2010), if Zn^{2+} could bind independently within each monomer, then the Zn^{2+} effects observed in the WT–H140A/H193A tandem dimer (Fig. 9) would be expected to be more profound. In contrast, this construct was nearly as insensitive to Zn^{2+} as the double mutant that lacks both His (H140A/H193A).

Since Zn^{2+} effects do not saturate at achievable concentrations, distinguishing differential binding affinity from differential efficacy at distinct sites is not straightforward. Nevertheless, some conclusions appear warranted. When Zn^{2+} binds either to His^{140} (in H193A) or His^{193} (in H140A) the g_H–V relationship shifts, although the shift is greater at any given $[Zn^{2+}]$ when Zn^{2+} binds at His^{193} (in H140A or H193A–H140A tandem). This result suggests that Zn^{2+} exerts a stronger effect on the voltage sensor of the proton channel when bound to His^{193} than to His^{140}. However, it is also possible that the affinity of Zn^{2+} is greater for His^{193} than for His^{140}.

Interpreting Zn^{2+} effects on the shift of the g_H–V relationship and slowing of τ_{act} is further complicated by the interrelatedness of these parameters. If the channel opening rate is decreased, the g_H–V relationship will shift positively, because the open probability will decrease at all potentials. Electrostatic effects generally shift voltage-dependent parameters along the voltage axis (Frankenhaeuser & Hodgkin, 1957; Hille, 2001; Elinder & Åhrem, 2004); in the simplest form of this type of mechanism, all parameters shift equally. However, the slowing of τ_{act} in proton channels by Zn^{2+} not only exceeds that predicted from the shift of the g_H–V relationship, but results in τ_{act} values at high Zn^{2+} that are slower than at any voltage without Zn^{2+} (Cherny & DeCoursey, 1999). It appears that Zn^{2+} slows channel opening by a distinct mechanism, and the data presented here indicate that this slowing effect occurs when Zn^{2+} binds to His residues. That no slowing was seen in H140A/H193A suggests that virtually the entire slowing effect can be attributed to Zn^{2+} binding to His^{140} and His^{193}. In addition, because the rank order of sensitivity to Zn^{2+} effects is different among the constructs tested for slowing and shift of the g_H–V relationship, these effects are, at least to some extent, separable.

The slowing of channel opening in the constructs tested (Fig. 9*B*) supports the hypothesis that the dimer interface allows His^{140} and His^{193} from each monomer to pair with the corresponding His from the other monomer to form a Zn^{2+} binding site. Profound slowing by Zn^{2+} occurs when all four His residues are present in the dimer (WT and WT–WT tandem). Moderate slowing also occurs when a single His residue is present in each monomer (H140A, H193A or H193A–H140A tandem dimer). The slowing of τ_{act} by Zn^{2+} was significantly weaker than WT in either single mutant, indicating that both His residues contribute to the slowing of channel opening. The weak but distinct slowing in the H193A–H140A tandem dimer might reflect coordination of Zn^{2+} between dissimilar His or between His^{193} and Glu^{192} or Glu^{196} in the opposite monomer. Glu^{192} and Glu^{196} are 9 Å and 11 Å, respectively, from His^{193} in the model, but they are in the flexible S3–S4 linker and thus might approach more closely. Remarkably, there was no slowing of τ_{act} in the WT–H140A/H193A tandem dimer. Taken together, these data suggest that when Zn^{2+} binds to His^{140} or His^{193} residues at the interface between monomers, neither monomeric channel can undergo the physical movement required for opening. Zn^{2+} may retard the movement of one monomer relative to the other during gating. Alternatively, Zn^{2+} may constrain the dimer in a conformation from which it cannot open.

The double His mutant H140A/H193A exhibited essentially no slowing by Zn^{2+} although a weak but distinct shift of the g_H–V relationship remained. The shift may reflect non-specific divalent cation effects or binding to residues on the channel other than His. In enzymes containing structural or catalytic Zn^{2+}, three or four amino acids (His, Cys, Glu or Asp) coordinate the Zn^{2+} (Vallee & Auld, 1990; Alberts *et al.* 1998). Of course, Zn^{2+} binding to the proton channel is neither structural nor catalytic and is rapidly reversible and consequently, a formal binding site is not expected.

Conformational changes during gating are unlikely to bring His^{140} and His^{193} closer together in the monomer

The homology model in Fig. 1 was based on what is presumed to be an open conformation of K^+ channels (Jiang *et al.* 2003*a*; Long *et al.* 2007). Closing of K^+ channels is thought to involve inward motion of S4, changing its orientation relative to other parts of the voltage-sensing domain (VSD; the S1–S4 complex) (Bezanilla, 2000; Jiang

et al. 2003*b*; Starace & Bezanilla, 2004; Tombola *et al*. 2006; Swartz, 2008). Roughly analogous motion of S4 in H_V1 is suggested by recent studies (Gonzalez *et al*. 2010; Tombola *et al*. 2010), although evidence that truncation of the C-terminus between the second and third Arg residues in S4 did not abolish proton selectivity or gating raises questions about the extent of similarity (Sakata *et al*. 2010). Positioned within a long helix, His^{140} is probably stationary. The kink in the S3 helix might allow His^{193} to swing toward the S2 helix and His^{140}, but the length of the S3b helix probably precludes an approach close enough for intramonomer Zn^{2+} binding. A model of the closed state of Kv1.2 (Pathak *et al*. 2007) does not show any significant decrease in the intramonomer distance between residues in positions homologous to those of His^{140} and His^{193}. This buttresses the idea that the H_V1 monomer does not support tight Zn^{2+} binding. In the dimer, conformational rearrangements (caused by S4 motion, for example) could orient the His pairs more favourably for *inter*-monomer Zn^{2+} binding in the closed, rather than in the open conformation, which would be consistent with the preferential effect of Zn^{2+} on channel opening over closing (Cherny & DeCoursey, 1999; Elinder & Åhrem, 2004).

Comparison of the proposed dimer interface with previous models

The dimer interface in Fig. 1*B*, which is supported by the Zn^{2+} studies, differs from previous proposals. FRET studies in the *Ciona* proton channel indicated 42 Å between corresponding Ser^{242} residues in the dimer (Koch *et al*. 2008), which like His^{193} in the human channel, is located in the S3–S4 linker. A study of H_V1 based on a series of Cys mutants led to a topological model (Lee *et al*. 2008) with a dimer interface different from that in Fig. 1*B*, in which the two His^{193} are far apart. However, in that study, distinct cross-links were also detected at position 194 in H_V1, at the tip of the voltage-sensor paddle (Lee *et al*. 2008), which indicates that His^{193} residues from each monomer are sometimes in close proximity. All of these observations can be reconciled if the proton channel dimer is loosely organized and occasionally samples alternative associations. This idea is supported by the fact that the channel appears as a monomer in Western blots (Ramsey *et al*. 2006; Koch *et al*. 2008; Lee *et al*. 2008, 2009; Capasso *et al*. 2010). Configurations in which His residues from both monomers approach each other may not occur frequently, but when they do, the opportunity for Zn^{2+} to bind exists. Zn^{2+} binding may then constrain the dimer in a conformation that precludes channel opening. Solving the crystal structure (Lee *et al*. 2009; Li *et al*. 2009) might shed light on these possibilities, but it may simply illustrate one of many possible orientations, or perhaps H_V1 will crystallize as a monomer. An alternative possibility that cannot be ruled out is that when the H_V1 dimer adopts a conformation with close apposition of S1 regions as proposed by Lee *et al*. (2009), Zn^{2+} binds between His residues exposed at the edges of dimers, promoting tetramer formation. Evidence consistent with tetramer or higher order polymer formation at least under specific conditions has been observed (Lee *et al*. 2009).

The C-terminus of H_V1 was crystallized recently, and structural changes were observed at different pH values (Li *et al*. 2010). Given that both the WT–WT tandem dimer (in which coiled-coil interaction along the entire C-termini may be disrupted by linking N- and C-termini together) and constructs lacking the C-terminus altogether, such as $H_V1\Delta C$, appeared to have normal pH dependence (Koch *et al*. 2008; Sakata *et al*. 2010), it seems unlikely that the pH dependence of gating resides in the C-terminus.

The enhanced gating mode does not reflect monomer–dimer interconversion

During the respiratory burst in neutrophils and eosinophils that accompanies phagocytosis and reflects NADPH oxidase activation, proton channels exhibit profoundly enhanced gating (Bánfi *et al*. 1999; DeCoursey *et al*. 2000). The enhanced gating strongly promotes proton channel opening and was predicted by modelling to improve the efficiency of NADPH oxidase by limiting the depolarization required to open enough proton channels to compensate for the electrogenic activity of the oxidase (Murphy & DeCoursey, 2006). Depolarization directly inhibits NADPH oxidase activity (DeCoursey *et al*. 2003; Petheő & Demaurex, 2005). Koch *et al*. (2008) speculated that the conversion of phagocyte proton channels to the 'enhanced gating mode' might reflect interconversion between monomeric and dimeric channel arrangements. As Zn^{2+} binds with high affinity between monomers in the dimer, but weakly to monomeric proton channels, one would predict different Zn^{2+} sensitivity of the two modes of gating. However, in eosinophils, the Zn^{2+} sensitivity of the proton channel in resting and enhanced gating modes is identical (DeCoursey *et al*. 2001). Since the monomeric proton channel ($H_V1\Delta C$) has distinctly weaker Zn^{2+} sensitivity, it appears that the phagocyte proton channel remains a dimer during enhanced gating. Enhanced gating can be explained by phosphorylation of the dimeric channel (Morgan *et al*. 2007; Musset *et al*. 2010).

Summary

Taken together, the evidence suggests profound inter-monomer interaction during opening in the dimeric voltage-gated proton channel, despite each monomer having a separate conduction pathway. Interaction between monomers during gating is suggested by the slower opening rate of the dimeric than the monomeric

channel, the higher activation energy of channel gating of the H_V1 dimer, and sigmoidal activation kinetics of the dimer compared with exponential kinetics of the monomer. Perhaps a concerted opening process occurs in the dimer. Alternatively, both monomers in the dimer may undergo identical gating movements as a prerequisite to conduction. Zn^{2+} slows channel opening most effectively when symmetrical His residues are available in both monomeric channels. As Zn^{2+} effects are weaker in monomeric than dimeric proton channels, the phagocyte proton channel in both resting and enhanced gating modes is evidently a dimer.

References

Alberts IL, Nadassy K & Wodak SJ (1998). Analysis of zinc binding sites in protein crystal structures. *Protein Sci* **7**, 1700–1716.

Bánfi B, Schrenzel J, Nüsse O, Lew DP, Ligeti E, Krause K-H & Demaurex N (1999). A novel H^+ conductance in eosinophils: unique characteristics and absence in chronic granulomatous disease. *J Exp Med* **190**, 183–194.

Bezanilla F (2000). The voltage sensor in voltage-dependent ion channels. *Physiol Rev* **80**, 555–592.

Byerly L, Meech R & Moody Jr W (1984). Rapidly activating hydrogen ion currents in perfused neurones of the snail, *Lymnaea stagnalis*. *J Physiol* **351**, 199–216.

Capasso M, Bhamrah MK, Henley T, Boyd RS, Langlais C, Cain K *et al*. (2010). HVCN1 modulates BCR signal strength via regulation of BCR-dependent generation of reactive oxygen species. *Nat Immunol* **11**, 265–272.

Cherny VV & DeCoursey TE (1999). pH-dependent inhibition of voltage-gated H^+ currents in rat alveolar epithelial cells by Zn^{2+} and other divalent cations. *J Gen Physiol* **114**, 819–838.

Cherny VV, Murphy R, Sokolov V, Levis RA & DeCoursey TE (2003). Properties of single voltage-gated proton channels in human eosinophils estimated by noise analysis and direct measurement. *J Gen Physiol* **121**, 615–628.

DeCoursey TE (1991). Hydrogen ion currents in rat alveolar epithelial cells. *Biophys J* **60**, 1243–1253.

DeCoursey TE (2003). Voltage-gated proton channels and other proton transfer pathways. *Physiol Rev* **83**, 475–579.

DeCoursey TE & Cherny VV (1994). Voltage-activated hydrogen ion currents. *J Membr Biol* **141**, 203–223.

DeCoursey TE & Cherny VV (1995). Voltage-activated proton currents in membrane patches of rat alveolar epithelial cells. *J Physiol* **489**, 299–307.

DeCoursey TE & Cherny VV (1998). Temperature dependence of voltage-gated H^+ currents in human neutrophils, rat alveolar epithelial cells, and mammalian phagocytes. *J Gen Physiol* **112**, 503–522.

DeCoursey TE, Cherny VV, DeCoursey AG, Xu W & Thomas LL (2001). Interactions between NADPH oxidase-related proton and electron currents in human eosinophils. *J Physiol* **535**, 767–781.

DeCoursey TE, Cherny VV, Zhou W & Thomas LL (2000). Simultaneous activation of NADPH oxidase-related proton and electron currents in human neutrophils. *Proc Natl Acad Sci U S A* **97**, 6885–6889.

DeCoursey TE & Ligeti E (2005). Regulation and termination of NADPH oxidase activity. *Cell Mol Life Sci* **62**, 2173–2193.

DeCoursey TE, Morgan D & Cherny VV (2003). The voltage dependence of NADPH oxidase reveals why phagocytes need proton channels. *Nature* **422**, 531–534.

Demaurex N, Grinstein S, Jaconi M, Schlegel W, Lew DP & Krause KH (1993). Proton currents in human granulocytes: regulation by membrane potential and intracellular pH. *J Physiol* **466**, 329–344.

Elinder F & Århem P (2004). Metal ion effects on ion channel gating. *Q Rev Biophys* **36**, 373–427.

Fernandez-Fuentes N, Zhai J & Fiser A (2006). ArchPRED: a template based loop structure prediction server. *Nucleic Acids Res* **34**, W173–W176.

Frankenhaeuser B & Hodgkin AL (1957). The action of calcium on the electrical properties of squid axons. *J Physiol* **137**, 218–244.

Gonzalez C, Koch HP, Drum BM & Larsson HP (2010). Strong cooperativity between subunits in voltage-gated proton channels. *Nat Struct Mol Biol* **17**, 51–56.

Hille B (2001). *Ion Channels of Excitable Membranes*, 3rd edn. Sinauer Associates, Inc., Sunderland, MA.

Hodgkin AL & Huxley AF (1952). A quantitative description of membrane current and its application to conduction and excitation in nerve. *J Physiol* **117**, 500–544.

Horrigan FT, Cui J & Aldrich RW (1999). Allosteric voltage gating of potassium channels I. Mslo ionic currents in the absence of Ca^{2+}. *J Gen Physiol* **114**, 277–304.

Humphrey W, Dalke A & Schulten K (1996). VMD: visual molecular dynamics. *J Mol Graph* **14**, 33–38.

Jiang Y, Lee A, Chen J, Ruta V, Cadene M, Chait BT & MacKinnon R (2003*a*). X-ray structure of a voltage-dependent K^+ channel. *Nature* **423**, 33–41.

Jiang Y, Ruta V, Chen J, Lee A & MacKinnon R (2003*b*). The principle of gating charge movement in a voltage-dependent K^+ channel. *Nature* **423**, 42–48.

Kapus A, Romanek R, Qu AY, Rotstein OD & Grinstein S (1993). A pH-sensitive and voltage-dependent proton conductance in the plasma membrane of macrophages. *J Gen Physiol* **102**, 729–760.

Koch HP, Kurokawa T, Okochi Y, Sasaki M, Okamura Y & Larsson HP (2008). Multimeric nature of voltage-gated proton channels. *Proc Natl Acad Sci U S A* **105**, 9111–9116.

Kuno M, Ando H, Morihata H, Sakai H, Mori H, Sawada M & Oiki S (2009). Temperature dependence of proton permeation through a voltage-gated proton channel. *J Gen Physiol* **134**, 191–205.

Laskowski RA, MacArthur MW, Moss DS & Thornton JM (1993). PROCHECK: a program to check the stereochemical quality of protein structures. *J Appl Cryst* **26**, 283–291.

Lee S-Y, Letts JA & MacKinnon R (2008). Dimeric subunit stoichiometry of the human voltage-dependent proton channel Hv1. *Proc Natl Acad Sci U S A* **105**, 7692–7695.

Lee S-Y, Letts JA & Mackinnon R (2009). Functional reconstitution of purified human Hv1 H^+ channels. *J Mol Biol* **387**, 1055–1060.

Li SJ, Zhao Q, Zhou Q, Unno H, Zhai Y & Sun F (2010). The role and structure of the carboxyl-terminal domain of the human voltage-gated proton channel Hv1. *J Biol Chem* (in press).

Li SJ, Zhao Q, Zhou Q & Zhai Y (2009). Expression, purification, crystallization and preliminary crystallographic study of the carboxyl-terminal domain of the human voltage-gated proton channel Hv1. *Acta Crystallogr Sect F Struct Biol Cryst Commun* **65**, 279–281.

Lomize MA, Lomize AL, Pogozheva ID & Mosberg HI (2006). OPM: orientations of proteins in membranes database. *Bioinformatics* **22**, 623–625.

Long SB, Tao X, Campbell EB & MacKinnon R (2007). Atomic structure of a voltage-dependent K^+ channel in a lipid membrane-like environment. *Nature* **450**, 376–382.

Mahaut-Smith M. (1989). The effect of zinc on calcium and hydrogen ion currents in intact snail neurones. *J Exp Biol* **145**, 455–464.

Morgan D, Cherny VV, Finnegan A, Bollinger J, Gelb MH & DeCoursey TE (2007). Sustained activation of proton channels and NADPH oxidase in human eosinophils and murine granulocytes requires PKC but not $cPLA_2\alpha$ activity. *J Physiol* **579**, 327–344.

Murphy R & DeCoursey TE (2006). Charge compensation during the phagocyte respiratory burst. *Biochim Biophys Acta* **1757**, 996–1011.

Musset B, Capasso M, Cherny VV, Morgan D, Bhamrah M, Dyer MJS & DeCoursey TE (2010). Identification of Thr^{29} as a critical phosphorylation site that activates the human proton channel *Hvcn1* in leukocytes. *J Biol Chem* **285**, 5117–5121.

Musset B, Cherny VV, Morgan D, Okamura Y, Ramsey IS, Clapham DE & DeCoursey TE (2008). Detailed comparison of expressed and native voltage-gated proton channel currents. *J Physiol* **586**, 2477–2486.

Pathak MM, Yarov-Yarovoy V, Agarwal G, Roux B, Barth P, Kohout S, Tombola F, Isacoff EY (2007). Closing in on the resting state of the Shaker K^+ channel. *Neuron* **56**, 124–140.

Petheő GL & Demaurex N (2005). Voltage- and NADPH-dependence of electron currents generated by the phagocytic NADPH oxidase. *Biochem J* **388**, 485–491.

Ramsey IS, Moran MM, Chong JA & Clapham DE (2006). A voltage-gated proton-selective channel lacking the pore domain. *Nature* **440**, 1213–1216.

Sakata S, Kurokawa T, Nørholm MHH, Takagi M, Okochi Y, von Heijne G & Okamura Y (2010). Functionality of the voltage-gated proton channel truncated in S4. *Proc Natl Acad Sci U S A* **107**, 2313–2318.

Sasaki M, Takagi M & Okamura Y (2006). A voltage sensor-domain protein is a voltage-gated proton channel. *Science* **312**, 589–592.

Sigworth FJ (1993). Voltage gating of ion channels. *Q Rev Biophys* **27**, 1–40.

Starace DM & Bezanilla F (2004). A proton pore in a potassium channel voltage sensor reveals a focused electric field. *Nature* **427**, 548–553.

Swartz KJ (2008). Sensing voltage across lipid membranes. *Nature* **456**, 891–897.

Tombola F, Pathak MM & Isacoff EY (2006). How does voltage open an ion channel? *Annu Rev Cell Dev Biol* **22**, 23–52.

Tombola F, Ulbrich MH & Isacoff EY (2008). The voltage-gated proton channel H_V1 has two pores, each controlled by one voltage sensor. *Neuron* **58**, 546–556.

Tombola F, Ulbrich MH, Kohout SC & Isacoff EY (2010). The opening of the two pores of the Hv1 voltage-gated proton channel is tuned by cooperativity. *Nat Struct Mol Biol* **17**, 44–50.

Tovchigrechko A & Vakser IA (2006). GRAMM-X public web server for protein-protein docking. *Nucleic Acids Res* **34**, W310–W314.

Vallee BL & Auld DS (1990). Zinc coordination, function, and structure of zinc enzymes and other proteins. *Biochemistry* **29**, 5647–5659.

Zhang Y (2008). I-TASSER server for protein 3D structure prediction. *BMC Bioinformatics* **9**, 40.

Author contributions

S.M.E.S., B.M., V.V.C., S.R. and T.E.D. contributed to conception and design; S.M.E.S., S.S. and S.R. contributed new tools; S.M.E.S. built the molecular model; B.M., V.V.C. and D.M. collected, analysed and interpreted data. T.E.D. wrote the paper; all authors critiqued the manuscript and approved the final version. Patch clamp studies were done at Rush University, constructs were generated at the University of Chicago and Emory University, molecular modelling was done at Emory University.

Acknowledgements

We thank I. Scott Ramsey and David E. Clapham for providing $H_V1\Delta C$ plasmid, and Tatiana Iastrebova for technical assistance. This work was supported by the Professor Adolf Schmidtmann Stiftung (B.M.), by NIDDK (DK-075706 to S.R.), by the Heart, Lung and Blood Institutes of Health (HL-61437 to T.E.D.) and by the National Science Foundation (T.E.D. and S.S.).